8-2013

Crystal Structure of the Ubiquitin-like Small Archaeal Modifier Protein 2 From Haloferax Volcanii

Yunfeng Li
University of Connecticut School of Medicine and Dentistry

Mark W. Maciejewski
University of Connecticut School of Medicine and Dentistry

Kai Jin
University of Connecticut School of Medicine and Dentistry

Yuhang Zhang
University of Connecticut School of Medicine and Dentistry

Bing Hao
University of Connecticut School of Medicine and Dentistry

THE PROTEIN SOCIETY

Crystal structure of the ubiquitin-like small archaeal modifier protein 2 from *Haloferax volcanii*

Yunfeng Li,[1] Mark W. Maciejewski,[1] Jonathan Martin,[2] Kai Jin,[1] Yuhang Zhang,[1] Julie A. Maupin-Furlow,[2] and Bing Hao[1]*

[1]Department of Molecular, Microbial, and Structural Biology, University of Connecticut Health Center, Farmington, Connecticut 06030

[2]Department of Microbiology and Cell Science, University of Florida, Gainesville, Florida 32611

Accepted 25 June 2013
DOI: 10.1002/pro.2305
Published online 2 July 2013 proteinscience.org

Abstract: The discovery of ubiquitin-like small archaeal modifier protein 2 (SAMP2) that forms covalent polymeric chains in *Haloferax volcanii* has generated tremendous interest in the function and regulation of this protein. At present, it remains unclear whether the *Hfx. volcanii* modifier protein SAMP1 has such polyubiquitinating-like activity. Although SAMP1 and SAMP2 use the same conjugation machinery to modify their target proteins, each can impart distinct functional consequences. To better understand the mechanism of SAMP2 conjugation, we have sought to characterize the biophysical and structural properties of the protein from *Hfx. volcanii*. SAMP2 is only partially structured under mesohalic solution conditions and adopts a well-folded compact conformation in the presence of 2.5*M* of NaCl. Its 2.3-Å-resolution crystal structure reveals a characteristic α/β central core domain and a unique β-hinge motif. This motif anchors an unusual C-terminal extension comprising the diglycine tail as well as two lysine residues that can potentially serve to interlink SAMP2 moieties. Mutational alternation of the structural malleability of this β-hinge motif essentially abolishes the conjugation activity of SAMP2 *in vivo*. In addition, NMR structural studies of the putative ubiquitin-like protein HVO_2177 from *Hfx. volcanii* show that like SAMP1, HVO_2177 forms a classic β-grasp fold in a salt-independent manner. These results provide insights into the structure–function relationship of sampylating proteins of fundamental importance in post-translational protein modification and environmental cues in Archaea.

Keywords: archaea; ubiquitin-like proteins; protein conjugation; sulfur transfer

Introduction

Conjugation of ubiquitin and ubiquitin-like (Ubl) polypeptide modifiers to various macromolecules is involved in the regulation of a diverse set of cellular processes in eukaryotic cells, including DNA repair, signal transduction, cell division, translation, autophagy, and proteasome-mediated proteolysis.[1–4] Covalent Ubl modifications can alter many functions of target proteins, including enzyme activity, protein stability, subcellular localization, and the ability to interact with other proteins. The dysregulation of Ubl-substrate modification and mutations in the Ubl-conjugation pathways have increasingly been implicated in the etiology and/or progression of a number of human diseases.[5,6] All the structurally characterized eukaryotic Ubls share the ubiquitin fold that consists of two conserved features: the so-

Grant sponsor: National Institutes of Health; Grant number: R01 GM099948; Grant sponsor: American Heart Association SDG; Grant number: 10SDG2640098; Grant sponsor: The U.S. Department of Energy, Office of Science, Office of Basic Energy Sciences under Award Number; Grant number: DE-FG02–05ER15650.

*Correspondence to: Bing Hao, Department of Molecular, Microbial and Structural Biology, University of Connecticut Health Center, Farmington, CT 06030-3305.
E-mail: bhao@uchc.edu

called β-grasp global core comprising a four- or five-stranded mixed β-sheet and an α-helix, in addition to a flexible C-terminal tail terminating with a glycyl–glycine motif.[7,8] The β-grasp fold creates a highly stable cooperative tertiary structure and is often resistant to environmental perturbation such as heat.[9] Through a C-terminal glycine residue, Ubl proteins become attached via an isopeptide bond to the ϵ-amino group of the side chain of lysine residues in protein targets. This conjugation reaction is generally catalyzed by a highly regulated three-step enzymatic cascade involving the sequential actions of an E1-activating enzyme, an E2-conjugating enzyme and an E3 protein ligase.[1,10]

Although the continuing discovery of new Ubl substrates has greatly expanded the functional diversity of Ubl pathways in eukaryotic cellular homeostasis and physiology, the presence of proteasomes in many prokaryotes[11,12] has generated tremendous interest in identifying such Ubl protein modification systems in archaea and bacteria. *Mycobacterium tuberculosis* Pup is the first known prokaryotic small modifier protein that can initiate the selective turnover of unwanted proteins by a bacterial proteasome in a manner akin to Ub-mediated proteolysis in eukaryotes.[13] However, Pup does not have a canonical ubiquitin fold and is in fact intrinsically disordered.[14–16] Although Pup has a glycine–glycine motif penultimate to its C-terminal residue, pupylation proceeds by different conjugation chemistry.[17–20] The C-terminal residue of Pup is a glutamine that is first deamidated by the Dop deamidase, and the deamidated Pup is then isopeptide-linked via the resulting glutamic acid γ-carboxyl group to lysine residues of target proteins, a reaction catalyzed by a glutamine synthetase-like PafA ligase. On the other hand, comparative genomic and biochemical studies have identified numerous β-grasp domain proteins in both bacteria and archaea.[21,22] For example, the structurally β-grasp-related ThiS[23] and MoaD[24] of *Escherichia coli* serve as sulfur carriers in thiamine and molybdopterin biosynthetic pathways in association with the E1-related enzymes ThiF and MoaE, respectively. Increasing evidence suggests that these types of sulfur transfer pathways or related enzymes were precursors of the eukaryotic ubiquitin system. This notion is supported by the finding that the ubiquitin-related modifier-1 (Urm1) functions as a sulfur carrier in thiolation of yeast transfer RNA and can also be ligated to a substrate protein via an exposed diglycine sequence protruding from its β-grasp fold.[25–27] Thus, Urm1 likely represents an evolutionary bridge between the ancient roles of Ubl proteins in sulfur chemistry and their advanced roles in protein conjugation.

Sampylation is a newly discovered prokaryotic protein-tagging system with parallels to the ubiquitin conjugation system and provides a direct link between protein modification and sulfur transfer in *Archaea* species such as *Haloferax volcanii*.[28,29] The small archaeal modifer protein 1 (SAMP1) and 2 (SAMP2) are involved in sulfur transfer during molybdenum cofactor biosynthesis and tRNA thiolation much like MoaD and Urm1, respectively.[30] Meanwhile, SAMP1 and SAMP2 have been demonstrated to form covalent conjugates with their substrate proteins through an isopeptide linkage via their C-terminal diglycine motif in a streamlined archaeal E1-dependent pathway.[30–32] SAMP2 also forms homo-conjugates through the intermolecular isopeptide bond between the C-terminal glycine and the Lys58 side chain, a feature that likely resembles polyubiquitination. Conjugation by SAMP1 and SAMP2 is growth condition-specific and likely occurs in response to environmental cue(s). Recently, the NMR structure of *Methanosarcina acetivorans* SAMP1[33] and the crystal structure of *Hfx. volcanii* SAMP1[34] have been reported. SAMP1 possesses a classic β-grasp fold that is similar to that of most Ubl proteins. To better understand the archaeal sampylation process and the structural principle underlying poly-SAMP2 conjugation activity, we have determined the atomic structures of SAMP2 and the putative Ubl protein HVO_2177[31] from *Hfx. volcanii*. Similar to SAMP1, HVO_2177 share significant structural similarities to other known Ubl proteins. Interestingly, SAMP2 forms a β-strand-interchanged dimer in the crystalline state, whereas the protein is a monomer in solution. Circular dichroism (CD) measurements indicate that SAMP2 is partially unfolded at low ionic strength and undergoes a β-hinge conformational switch as the ionic strength of a buffer is increased by adding sodium chloride from 200 m*M* to 2*M*. Mutagenesis studies suggest that this β-hinge region plays a crucial role in maintenance of SAMP2 conjugation activity. These results point to a conformational control of sampylating activity and suggest a stabilizing mechanism by which SAMP2 maintains its functional characteristics under extremely high-salt conditions in halophilic archaea.

Results

Structure determination of SAMP2

The crystal structure of SAMP2 was determined at 2.3-Å resolution by molecular replacement using a chemical shift (CS)-based Rosetta generated SAMP2 model. Crystallization trials yielded well-diffracting crystals of the native SAMP2 protein but not its selenomethionine (SeMet)-substituted variants. We were not able to identify its structural phases using the molecular replacement method with known Ubl structures. We thus sought to construct a high-resolution NMR-based structural model of SAMP2 to solve the phase problem. The proton–nitrogen heteronuclear single-quantum coherence (HSQC) spectrum of

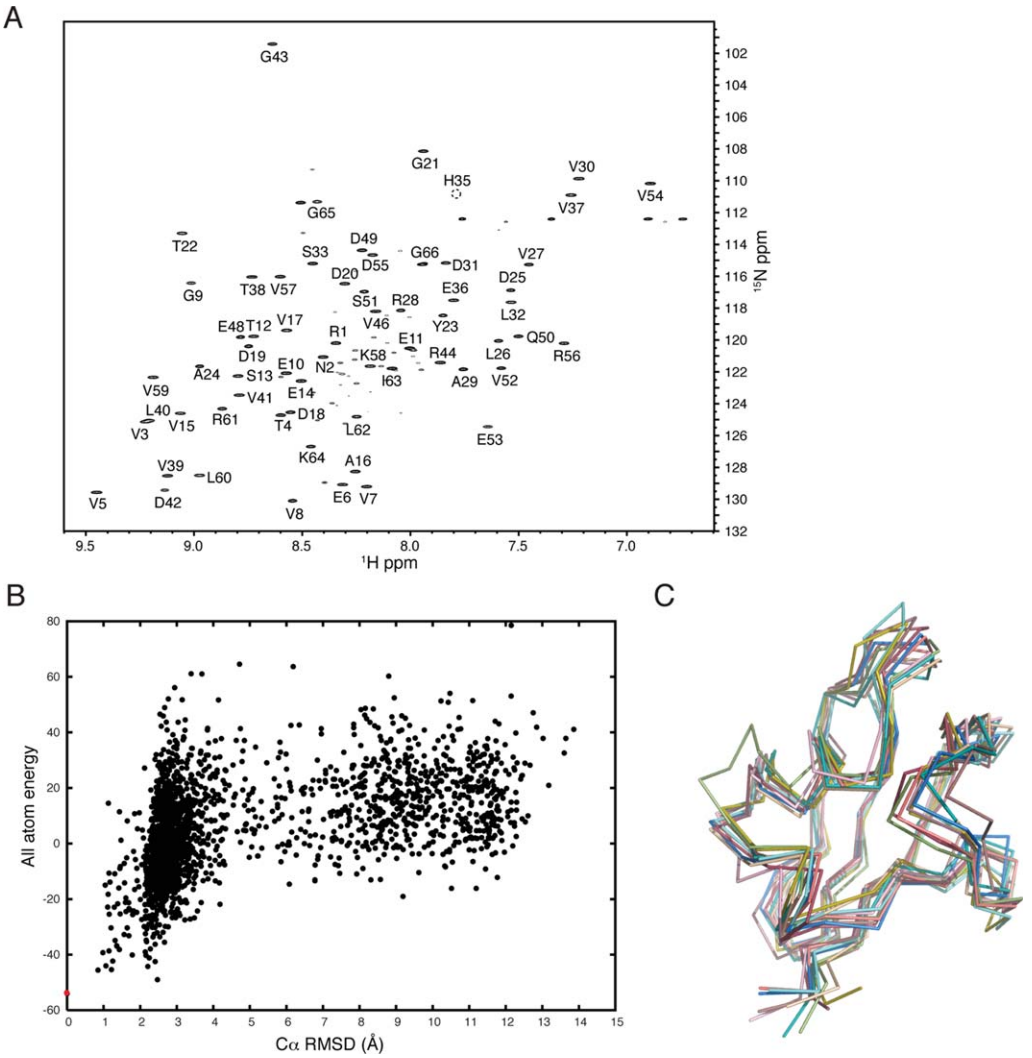

Figure 1. Generation of the 3D models of SAMP2 using CS-Rosetta. (A) ^{1}H, ^{15}N-HSQC spectrum of SAMP2 in Na-K phosphate buffer at 25°C. (B) Energy of the CS-Rosetta-generated models versus rmsd to the lowest energy structure (red dot). Around 2000 models of SAMP2 were generated of which 10 with the lowest energies were analyzed. (C) Superposition of the top 10 CS-Rosetta models with the lowest energies.

SAMP2 is shown in Figure 1(A). Each peak or resonance in this spectrum originates from a covalently linked proton–nitrogen pair within the protein, either along the polypeptide backbone or in the side-chain groups. Complete sequence-specific resonance could be assigned as indicated in the spectrum, and was derived from triple resonance NMR data in combination with backbone amide proton NOESY spectra. The NMR CS data were then used for CS-Rosetta structure calculation.[35] The CS-Rosetta models converged on a well-defined structure that closely resembles the β-grasp fold with the average Cα root-mean-square deviation (rmsd) of the 10 lowest-energy structures around 1.7 Å [Fig. 1(B,C)]. By using those structures as search models for molecular replacement, the initial phases were determined for the diffraction data of SAMP2. The resulting electron density maps show clear solvent boundaries and side-chain densities. We immediately noticed differences in the positioning of the C-terminal β-strand (residues, 53–66) between the CS-Rosetta model and the crystallographic map. The 14 residues in this β-strand were therefore removed from the model in subsequent refinement steps, and the resulting omit maps unambiguously confirmed the position of the β-hinge region in the SAMP2 model [Fig. 2(A)]. Iterative model building and crystallographic refinement resulted in a model with an R-factor of 21.5% and a free R-value of 25.4%, with all residues in allowed regions of the Ramachandran plot (Table I).

Novel structural fold of SAMP2

The secondary structure of SAMP2 consists of a pair of antiparallel β-strands, an α-helix, a 3_{10} helix, and three C-terminal β-strands [Fig. 2(B)]. The arrangement of these secondary structure elements and the

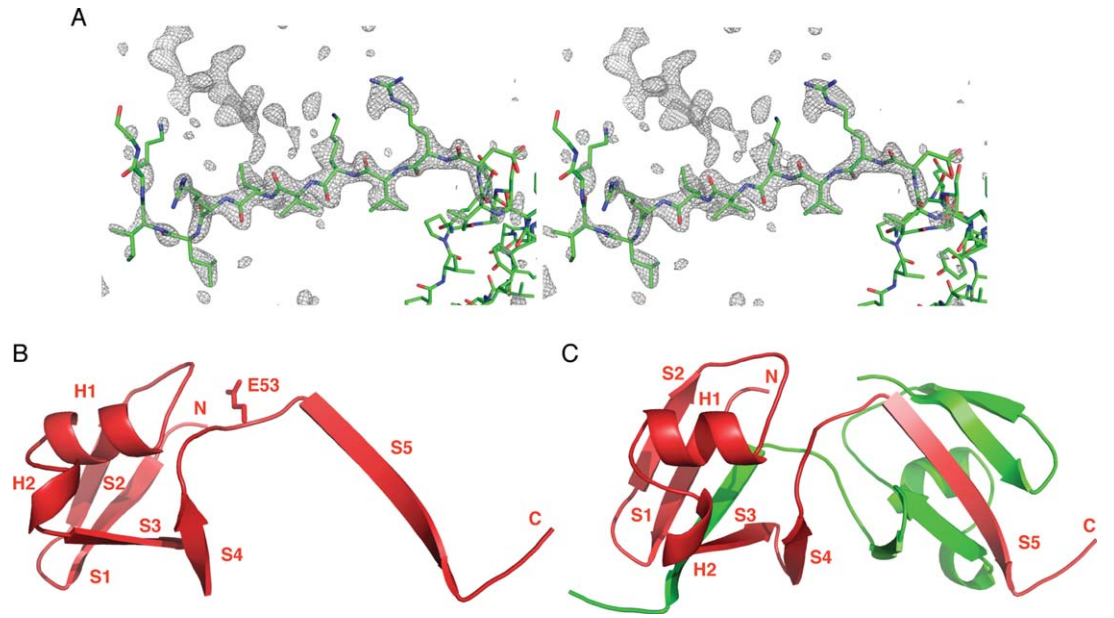

Figure 2. Overall structure of the *Hfx. volcanii* SAMP2 protein. (A) A stereo view of the representative Fo–Fc density map showing the region of the S5 strand of SAMP2. The map is contoured at 3.0σ. (B) Overall structure of SAMP2. Glu53 is shown as a stick model. (C) Ribbon diagram of two interlocked SAMP2 molecules created by the crystallographic twofold axis. The two molecules are colored red and green, respectively.

overall folding topology are similar to those of Ubl proteins,[7,8] SAMP1,[33,34] and HVO_2177 (see below). Each SAMP2 polypeptide is folded into two two-stranded antiparallel β-sheets (S1/S2 and S3/S4), abutted at the top by two helices (H1 and H2) to form a hydrophobic core. The most striking feature of this monomer fold is the C-terminal extension of the β-strand S5 and the diglycine motif, separate from the central core domain [Fig. 2(B)]. The Glu53 residue serves as the pivot point in the extended β-hinge conformation. Serendipitously, the two SAMP2 molecules associate to form an interlocked dimer with a crystallographic twofold axis in the crystalline state [Fig. 2(C)]. The extended S5 β-strand of one monomer packs against the S1 and S3 strands of the neighboring molecule to form an intermolecular five-stranded β-sheet. So far as we know, this type of β-strand interchange has not been seen before in Ubl proteins (see below). Moreover, ~3500 Å^2 (~31%) of the total solvent-accessible surface in each monomer is buried in the dimer interface, raising the possibility that the C-terminal extension may well affect the structural stability of the uncommon SAMP2 fold.

Table I. *X-ray Data Collection and Refinement Statistics for SAMP2*

Data collection	
Wavelength (Å)	1.075
Space group	*I*222
Cell dimensions (Å)	
a, *b*, *c* (Å)	24.6, 64.6, 104.6
α, β, γ (°)	90.0, 90.0, 90.0
Resolution (Å)	50.00–2.30 (2.34–2.30)
R_{sym} (%)	6.2 (15.6)
$I/\sigma I$)	43.4 (18.4)
Completeness (%)	99.0 (97.2)
Redundancy	12.6 (12.4)
Refinement	
Resolution (Å)	50.00–2.30
No. of reflections ($\|F\| > 0\sigma$)	3771
R-factor/R_{free}	21.5/25.4
Total protein atoms	493
Water molecules	34
B-factors (average) (Å^2)	
Protein	27.4
Water	32.0
rmsds	
Bond lengths (Å)	0.010
Bond angles (°)	1.214
Ramachandran (%)	
Within-favored	95.5
Within-allowed	100
Outliers	0

The number in parentheses is for the highest resolution shell.

Salt-induced folding of SAMP2

The β-hinge region is well ordered and has low-temperature factors in the crystal structure of SAMP2 [Fig. 2(A)]. The relative orientation of the C-terminal strand of the protein is imposed almost entirely through the loop conformation between the S4 and the S5 strands in the crystalline state. Given that SAMP2 was crystallized in high-salt conditions, we were interested in determining the extent to which ionic strength could influence the folding and stability of SAMP2 in the solution. On the basis of CD measurements at 4°C, SAMP2 is partially folded

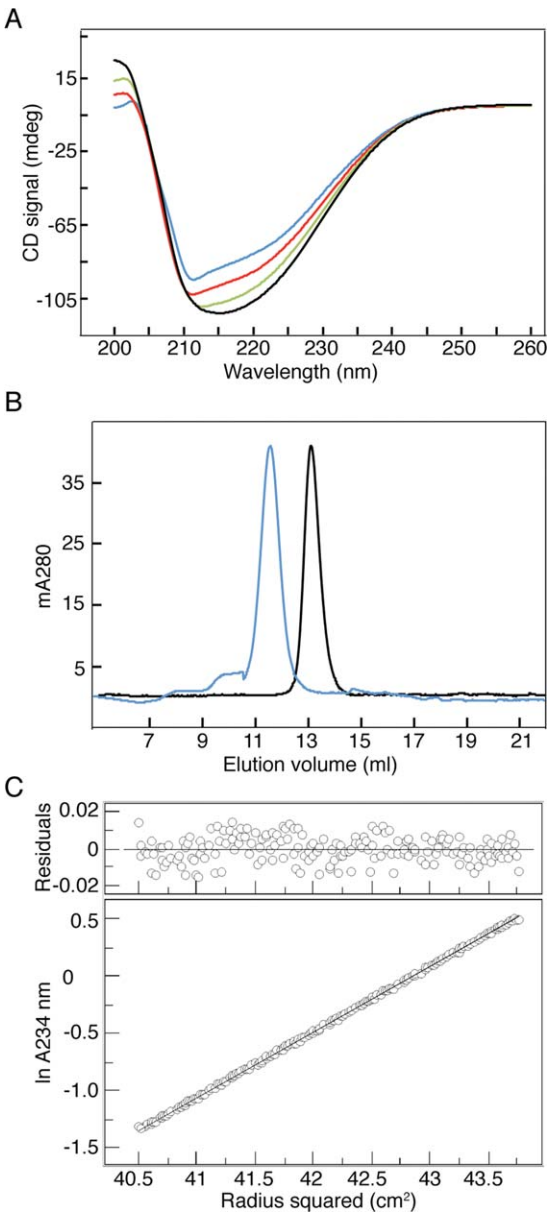

Figure 3. Effect of ionic strength on the folding and conformation of SAMP2. (A) CD spectra of SAMP2 at 4°C in 10 m*M* of Tris-HCl (pH 8.0) supplemented with 100 m*M* (blue), 500 m*M* (red), 1*M* (green), and 2.5*M* (black) NaCl. (B) Overlay of gel-filtration chromatography profiles of SAMP2 incubated in 20 m*M* of Tris-HCl (pH 8.0) supplemented with 200 m*M* (blue) and 2.5*M* (black) NaCl. (C) Representative sedimentation equilibrium data (34,000 rpm) for SAMP2 (250 μM) at 4°C in a buffer containing 20 m*M* of Tris-HCl (pH 8.0) and 2.5*M* of NaCl. The data fit closely to a monomer (Upper). The deviation in the data from the linear fit for a monomeric model is plotted.

in Tris buffer supplemented with 100 m*M* of NaCl [Fig. 3(A)]. CD spectra of SAMP2 in the presence of increasing concentrations of NaCl show strong negative bands around 210 and 220 nm [Fig. 3(A)]. This type of spectrum has been observed in mixed α/β-proteins and appears to represent the formation of native secondary structure in SAMP2. An isodichroic point observed in the far-UV CD spectra at 205 nm [Fig. 3(A)] suggests that the folding of SAMP2 is a simple two-state transition. A maximum increase in ellipticity and secondary structure contents was observed upon increasing the ionic strength to 2.5*M* of NaCl, similar to that used in the growth medium for halophilic archaea.[36] In contrast, alteration of ionic strength has no effect on the CD spectra of SAMP1 and HVO_2177 (data not shown). In addition, gel filtration chromatography of SAMP2 revealed a significantly longer retention time in the high-salt buffer [Fig. 3(B)], in keeping with salt-induced hydrophobic compaction and secondary structure formation. Nevertheless, SAMP2 is monomeric even at high ion strength buffer (up to 2.5*M* of NaCl) and high protein concentration (up to 800 μ*M*) as determined by sedimentation equilibrium experiments [Fig. 3(C)]. It is possible that SAMP2 undergoes a global conformational change induced by high ionic strength at its native conditions.

Functional role of the β-hinge region

As described above, SAMP2 contains the unique β-hinge motif that is important to properly orient the C-terminal extension of ~14 residues beyond the hydrophobic core of the protein. We hypothesized that the β-hinge flexibility may be an important determinant of the SAMP2 conformation that favors both substrate protein interactions and polysampylation. To directly test this hypothesis, we replaced Glu53, located at the pivot point of the S4–S5 loop in the protein, with alanine and glycine, respectively, to create the E53A and E53G mutants. Alanine was selected because of the small size of its methyl side chain that allows certain degree of conformational flexibility, whereas glycine was chosen because it lacks a side chain and thus would accommodate rotation of the C-terminal strand of the protein into a range of conformations.[37,38] Plasmids encoding Flag-tagged SAMP2 E53A and E53G were transformed into *Hfx. volcanii*. The two variant proteins were examined for their ability to be expressed and form protein conjugates as detected by immunoblotting using an α-Flag-specific antibody;[31] the polyvinylidene difluoride (PVDF) membranes were also stained with Ponceau S to ensure equal protein loading and transfer (data not shown). Both E53A and E53G were expressed at similar levels to the wild-type protein in the *Hfx. volcanii* strain grown on a complete medium containing 2.14*M* of NaCl (Fig. 4). Although the E53A substitution resulted in a modest reduction (~3-fold) relative to the wild type, the E53G mutation essentially abolished the sampylation reaction. We believe that the loss of SAMP2 conjugation activity originates from the effect of the Glu53-to-Gly substitution on the β-hinge conformation of the protein and support the notion that relative orientation of the C-terminal strand that

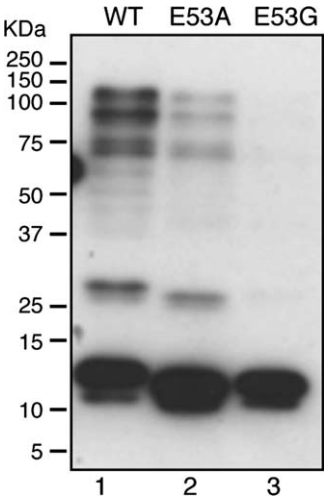

Figure 4. Effects of Glu53 mutation on levels of SAMP2-conjugates in *Hfx. volcanii* cells. SAMP2 and SAMP2 conjugates in wild-type and Glu53 mutant cells grown on complex medium were detected by immunoblotting with an anti-Flag antibody. The PVDF membranes were also stained with Ponceau S to confirm equal protein loading and transfer.

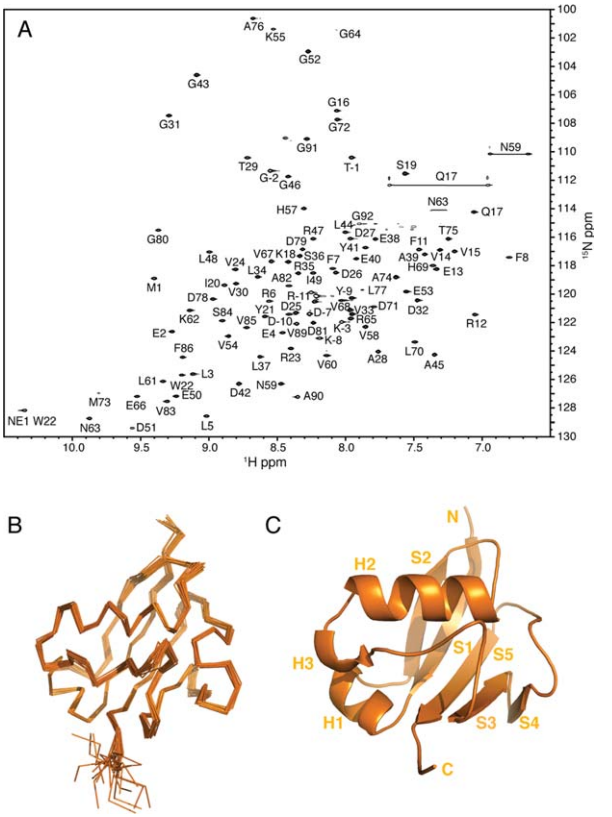

Figure 5. Overall structure of the *Hfx. volcanii* HVO_2177 protein. (A) ^{1}H, ^{15}N-HSQC spectrum of HVO_2177 showing selected assignments. (B) Stereo representation of a superposition of the backbone of the 20 lowest energy refined structures of HVO_2177. (C) Ribbon diagram of the lowest energy HVO_2177 structure.

bearing two lysine residues to the core is critical for SAMP2 conjugation activity. Nevertheless, the Glu53-to-Gly mutation can also induce global protein unfolding and/or impact a SAMP2–substrate interaction interface directly. Further study is required to clarify how altering the β-hinge conformation might lead to this phenotype.

Structure of Hfx. volcanii HVO_2177

We determined the structure of the putative Ubl protein HVO_2177 in *Hfx. volcanii* by NMR spectroscopy; the HVO_2177 protein expressed in this study represents residues 22–113 of the polypeptide deduced from DNA sequence spanning 2049666–2050007 of the *Hfx. volcanii* DS2 genome (GI: 292654178).[39] The HVO_2177 protein has a C-terminal diglycine motif and is predicted to possess a β-grasp fold similar to SAMP1 and SAMP2.[31] The ^{1}H-^{15}N HSQC spectra of HVO_2177 are shown in Figure 5(A). The CSs are well dispersed in both the ^{1}H and the ^{15}N dimensions and allow for almost complete sequence-specific backbone assignments of the protein using a standard set of triple-resonance NMR experiments. Secondary structure prediction based on the backbone ^{1}H, ^{15}N, and ^{13}C CSs using TALOS+[40] confirmed that the protein consists of five β-strands and two α-helices. Nuclear Overhauser effect (NOE) crosspeaks from the 3D NOESY spectra were used to generate 3421 distance restraints through automated assignment methods. CS data were used with TALOS+ to generate 164 dihedral angle restraints. CYANA[41] was used to generate 200 conformers of which the 20 with the lowest target function were refined in explicit solvent in CNS[42] to generate a well-defined ensemble with a backbone rmsd of 0.28 Å from the mean [Table II; Fig. 5(B,C)]. Sedimentation equilibrium experiments show that both HVO_2177 and SAMP1 sediment as discrete monomers (data not shown).

As expected, HVO_2177 adopts a global β-grasp fold [Fig. 5(C)]. HVO_2177 consists of a five-stranded-mixed β-sheet with the β2↑β1↓β5↓β3↑β4↓ topology that is same as SAMP1, as well as two α-helices and one 3_{10} helix flanking on the side of the β-sheet. Furthermore, HVO_2177 appears structurally more closely related to SAMP1[34] than SAMP2 [Fig. 6(A,B)]. SAMP1 shares 48% amino acid sequence identity with HVO_2177. In addition, SAMP1[34] and HVO_2177 share a similar tertiary structure with a Cα rmsd of 2.0 Å, indicating that the overall canonical β-grasp fold is preserved among Ubl proteins in halophilic archaea [Fig. 6(B)]. The only major structural difference lies in the region between the H3 helix and the S3 strand, with the well-defined H3 helix in SAMP1, whereas there is a crossover loop and a 3_{10} helix in this region of HVO_2177. Importantly, Lys4 is the only lysine residue of SAMP1 that could potentially form polymeric

Table II. *NMR Structural Statistics for the 20 Lowest Energy Structures of HVO_2177*

NMR restraints	
Total distance restraints	3421
Intraresidues	549
Sequential ($\|i-j\|=1$)	808
Short range ($\|i-j\|\leq 1$)	1357
Medium range ($1<\|i-j\|<5$)	640
Long range ($\|i-j\|\geq 5$)	1424
Dihedral angles restraints (φ and ψ)	164
Residual NOE violations	
Mean number >0.3 Å	3.5 ± 1.6
Mean number >0.5 Å	0
Average deviation from idealized geometry	
Bond lengths (Å)	0.0140 ± 0.0001
Bond angles (°)	1.02 ± 0.02
rmsds from mean	
Backbone atoms	0.28 ± 0.05
All heavy atoms	0.66 ± 0.06
Ramachandran (%)	
Within-favored	87.5
Within-allowed	95.2
Outliers	4.8

chains and this lysine aligns structurally with HVO_2177 Arg6. This could explain the observation that HVO_2177 lacks sampylating activity.[31]

Structural comparisons among Ubl proteins

In spite of only 22% sequence identity shared between SAMP1 and SAMP2 [Fig. 6(A)], these two proteins can be superposed with an rmsd of 1.5 Å for 49 out of 69 α-carbon atoms and with better superposition of the center core domain [Fig. 6(C)]. Apparently, SAMP2 replaces the H1 and H3 α-helices in SAMP1 with a 3_{10} helix to form a more compact core domain with the extended C-terminal β-stand and tail [Fig. 6(C)]. The presence of two lysine residues (Lys58 and Lys64) in this extension suggests that they are likely more accessible for modification than the only lysine residue Lys4 in SAMP1. It is also possible that the poly-SAMP2 chain displays significant structural differences from classic polyubiquitin chains linked by Lys48 or Lys63 of ubiquitin. Importantly, all three Ubl proteins, SAMP1, SAMP2, and HVO_2177, contain a conserved hydrophobic pocket that is responsible for ubiquitin recognition by other proteins [Fig. (6C,E)]. This hydrophobic patch is centered at Ile44 of ubiquitin, and the structurally equivalent residues in SAMP1 (Leu60), SAMP2 (Leu40), and HVO_2177 (Leu61) are positioned in a similar orientation as Ile44. This observation suggests that the conserved

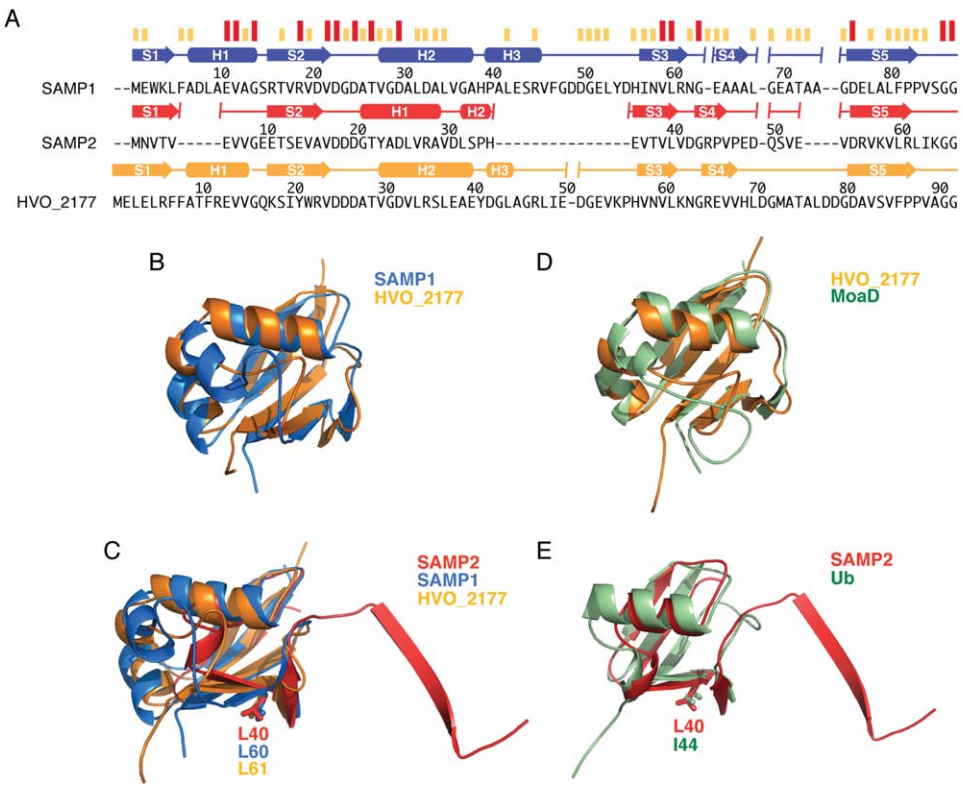

Figure 6. Sequence conservation and structure similarity among SAMP proteins and their homologues. (A) Sequence conservation and secondary-structure elements for SAMP1, SAMP2, and HVO_2177. Sequence conservation is shown as a bar graph, with red bars indicating identity among all three proteins. Secondary-structure assignments from the crystal (SAMP1[34] and SAMP2) and NMR (HVO_2177) structures are shown as cylinders (α-helices) and arrows (β-strands) colored in blue for SAMP1, red for SAMP2, and orange for HVO_2177. (B) Superposition of SAMP1 (blue; PDB ID: 3PO0) and HVO_2177 (orange). (C) Superposition of SAMP1 (blue), SAMP2 (red), and HVO_2177 (orange). (D) Superposition of HVO_2177 (orange) and *Pyrococcus furiosus* MoaD (green; PDB ID: 1VJK). (E) Superposition of SAMP2 (red) and *Homo sapiens* ubiquitin (green; PDB ID: 1UBQ).

Table III. *Structural Homologs of SAMP2 and HVO_2177*

PDB id	*Z*-score	rmsd (Å)	Protein
SAMP2			
1YIW	6.4	1.6	Chemically synthesized *H. sapiens* ubiquitin
1R4M	6.2	1.7	*H. sapiens* NEDD8
1UBQ	5.6	1.9	*H. sapiens* ubiquitin
3PO0	4.3	2.0	*Hfx. volcanii* SAMP1
1ZUD	3.1	2.3	*E. coli* ThiS
1V8C	3.0	7.4	*Thermus thermophilus* MoaD
3DWG	2.6	2.4	*M. tuberculosis* CysO
2L52	2.5	2.2	*Methanosarcina acetivorans* SAMP1 homolog
HVO_2177			
1V8C	12.5	1.6	*T. thermophilus* MoaD
2L52	12.1	2.0	*M. acetivorans* SAMP1 homolog
3PO0	11.3	2.2	*Hfx. volcanii* SAMP1
1VJK	10.8	2.0	*P. furiosus* MoaD
3DWG	10.7	2.8	*M. tuberculosis* CysO
2QJL	9.8	2.3	*Saccharomyces cerevisiae* Urm1
1UBQ	5.9	2.7	*H. sapiens* ubiquitin
1ZUD	5.6	2.1	*E. coli* ThiS

hydrophobic pocket also plays a role in regulation of protein–protein interactions by the sampylation or other pathways.

The structure homology searches of the Protein Data Bank using the Dali server[43] revealed unequivocal structural resemblance of HVO_2177 with more than 800 Ubl proteins, including Urm1, ubiquitin, and the bacterial sulfur carrier proteins MoaD, ThiS, and CysO [Table III; Fig. 6(D)]. The finding that HVO_2177 shows high structural similarity with sulfur transfer proteins is consistent with the predictions of HVO_2177 function based on comparative genomic and sequence analysis of all archaeal Ubl proteins.[29] In contrast, a similar homology search revealed that SAMP2 shares low structural similarity to a number of Ubls, likely owing to its peculiar β-hinge-containing topology [Table III; Fig. 6(E)]. Taken together, we conclude that SAMP2 represents a previously uncharacterized type of the Ubl fold.

Discussion

Sampylation by SAMP2 may target proteins for proteasome-mediated degradation in *Hfx. volcanii* through self-modification to form poly-SAMP chains much like eukaryotic ubiquitin and SUMO.[31] The structural and biochemical studies presented here will contribute to our current understanding of the regulatory and structural variations of Ubl proteins in halophilic archaea. We find that SAMP2 adopts an unusual configuration in which the C-terminal strand forms an open β-hinge motif, whereas SAMP1 and HVO_2177 retain the hallmark β-grasp fold. Considering that Pup is an intrinsically disordered protein bearing little sequence or structural resemblance to ubiquitin, it appears that prokaryotic polypeptide modifiers can adopt diverse conformations to exert phenotypic effects on a plethora of targets. The unique extended β-hinge conformation of SAMP2 leads us to posit that the two lysine sites in this region may play an important role in determining the substrate specificity of sampylation. We should emphasize that although SAMP2 forms a stable β-interchanged dimer in the crystalline state, sedimentation equilibrium experiments revealed a monomeric SAMP2 in solution regardless of ionic strength. In addition to crystal packing, the high protein concentration (80 mg mL^{-1}) used for crystallization could well contribute to dimer formation, given that the highest protein concentration used in sedimentation experiments was 5.8 mg mL^{-1}. It is thus possible that the β-hinge motif in SAMP2 is flexible and this flexibility allows the protein to have a more globular and compact fold in solution than in crystals. In fact, the interconversions between open and closed conformations could provide a structural basis for altering SAMP2 functional interactions with its target proteins. This notion is supported by site-directed mutagenesis studies, showing that the relative orientation and a certain degree of flexibility of the terminal strand are critical for SAMP2 conjugation activity.

We also find that SAMP2 is partially folded under normal conditions but forms a well-folded structural domain in the presence of 2.5*M* of NaCl, the natural growth environment of halophilic archaea. This finding suggests a possible mechanism for coordinated folding and structural rearrangements of SAMP2 in relation to environmental cues or interactions with substrate/partner proteins, consistent with the observations that the level of sampylation is closely regulated by growth condition.[31] In fact,

conformational variation is emerging as a widespread theme in eukaryotic Ubl conjugation cascades. For example, eukaryotic E1s and some E3s undergo domain rotations that are critical for their catalytic activities.[44,45] To our knowledge, we show for the first time that the polypeptide modifier itself undergoes conformation changes that could act to regulate its conjugation function and/or specificity. As a single member of the E1 family has been identified in *Hfx. volcanii*, and E2- and E3-like proteins are not predicted in the majority of archaeal genomes, the environment-sensitive folding of SAMP2 can provide an alternative means to regulate the structure, activity, interactions, location, and/or half-life of haloarchaeal proteins.

Materials and Methods

Cloning, expression, and protein purification

The *samp1* (HVO_2619), *samp2* (HVO_0202), and HVO_2177 genes were generated by PCR using genomic DNA isolated from *Hfx. volcanii* DS2 as template and cloned into a modified pET15b vector (EMD Millipore, Billerica, MA). The SAMP1 (residues, 1–87), SAMP2 (2–66), and HVO_2177 (24–113) proteins were expressed in *E. coli* and purified by Ni^{2+}-NTA affinity chromatography followed by TEV protease cleavage of the His_6 tag. These proteins were purified to homogeneity by sequential anion-exchange and gel filtration (SD75; GE Healthcare, Piscataway, NJ) chromatography. For crystallization, SAMP2 was concentrated to 80 mg mL^{-1} by ultrafiltration in 20 m*M* of HEPES (pH 7.4), 200 m*M* of NaCl. For NMR experiments, SAMP2 and HVO_2177 were expressed in M9 minimal media supplemented with $^{15}NH_4Cl$ and ^{13}C-glucose as the sole nitrogen and carbon sources, respectively. The ^{13}C, ^{15}N-labeled SAMP2, and HVO_2177 were purified as described above and concentrated to 1 m*M* in 25 m*M* of Na-K phosphate (pH 6.2 for SAMP2 and pH 7.2 for HVO_2177), 500 m*M* of NaCl, 0.2 m*M* of EDTA, 10% D_2O, and 0.02% NaN_3.

Crystallization and structure determination

Crystals were grown by the hanging-drop vapor diffusion method at 4°C. SAMP2 was crystallized from 100 m*M* *bis-tris*-propane-HCl (pH 6.8), 25–30% w/v PEG 400, 0.2*M* of $MgCl_2$, 0.1*M* of KCl. The crystals were flash-frozen in crystallization solution directly. Diffraction data were collected on the X29A beamline at the National Synchrotron Light Source (Brookhaven, NY), and reflection intensities were integrated and scaled using the HKL2000 suite.[46] Initial phases for SAMP2 were obtained with molecular replacement using the top 10 lowest-energy CS-Rosetta models (see below) as the search models with Phaser.[47] Iterative cycles of refinement in REFMAC with TLS[48] followed by manual rebuilding in Coot were carried out until no further improvement of the R_{free} factor was observed. X-ray data collections, phasing, and refinement statistics are summarized in Table I. Ramachandran statistics were calculated using Molprobity.[49] Molecular graphics were rendered using PyMOL (Delano Scientific LLC).

NMR measurements and structure calculations

NMR experiments were performed at 25°C on 600 and 800 MHz spectrometers (Agilent VNMRS) using the uniformly ^{13}C,^{15}N-labeled SAMP2, and HVO_2177 samples prepared as described above. The HVO_2177 sample was exchanged into D_2O by repeating cycles of concentrating and diluting in buffer made in D_2O; spectra collected in 100% D_2O are noted. 2D ^{15}N-^{1}H-HSQC, 2D HNCACO, 3D HNCACB, and 3D HNCO spectra were used for ^{1}H, ^{15}N, $^{13}C\alpha$, $^{13}C\beta$, and ^{13}C backbone resonance assignments. Side-chain Hα- and Hβ-assignments were obtained using a 3D HBHA(CO)NH spectra. Side-chain ^{1}H and ^{13}C resonance assignments were obtained using 3D H(CCCO)NH-TOCSY, (H)CC(CO)NH-TOCSY, and HCCH-TOCSY (D2O) spectra. Side-chain ^{1}H and ^{13}C resonance assignments for the aromatic rings of Trp, Tyr, Phe, and His were obtained using 2D (HB)CB(CGCD)HD, 2D aromatic ^{13}C-^{1}H-HSQC (D_2O), and 3D aromatic HCCH-TOCSY (D_2O) spectra. Distance restraints were obtained using 3D ^{13}C-edited NOESY-HSQC (D_2O), ^{15}N-edited NOESY-HSQC, and aromatic ^{13}C-edited NOESY-HSQC (D_2O) spectra with mixing times of 150 ms. All spectra were processed with the Rowland NMR Toolkit[50] and analyzed with the program XEASY.[51] For HVO_2177 structure calculation, NOE spectra were manually peak-picked and integrated in XEASY. The restraints for the backbone dihedral Phi and Psi angles were derived from the backbone resonance assignments using the TALOS+ program.[40] The NOE crosspeaks were assigned with automatic NOESY assignments using CYANA.[41] NOE assignments were manually verified and 200 preliminary structures determined with CYANA. The 20 structures with the lowest target function were further refined by short constrained molecular dynamic simulations in explicit solvent using CNS.[42] NMR-based restraints used for structure determination along with the structure refinement statistics are summarized in Table II.

SAMP2 tertiary structure prediction

The 3D models of SAMP2 were generated and rescored with CS-Rosetta[35] using the backbone ($^{13}C\alpha$, ^{13}C, ^{15}N, $^{1}H\alpha$, and $^{1}H_N$) and $^{13}C\beta$ NMR CS data as input. The structural calculations were run locally and generated 2168 candidate structures. The 1000 lowest energy structural models were

extracted to assess convergence. Of these, the top 10 lowest energy models all differ by <1.7 Å Cα RMSD from the model with lowest (rescored) energy.

Analytical ultracentrifugation

Sedimentation equilibrium measurements were carried out on a Beckman XL-A analytical ultracentrifuge (Beckman Coulter, Brea, CA) using an An-60 Ti rotor (Beckman Coulter, Brea, CA). Protein samples were dialyzed overnight against 20 m*M* of Tris-HCl (pH 8.0), 200 m*M* or 2.5*M* of NaCl, loaded at three initial concentrations for each sample (60–600 μ*M* for SAMP1, 80–800 μ*M* for SAMP2, and 70–700 μ*M* for HVO_2177) and analyzed at rotor speeds of 30,000 and 34,000 rpm at 4°C. Data were acquired at two wavelengths per rotor speed setting and processed globally for the best fit to a single-species model of absorbance versus radial distance by using Origin provided by the manufacturer. Solvent density and protein partial specific volume were calculated according to the solvent and protein composition, respectively.[52] Apparent molecular masses were within 10% of those calculated for an ideal monomer, with no systematic deviation of the residuals.

CD spectroscopy

CD measurements were carried out on an Aviv 410 CD spectrophotometer in 10 m*M* of Tris-HCl (pH 8.0) and varying concentrations of NaCl. Spectra were recorded as the average of five scans using a 5-s integration time at 1.0-nm wavelength increments. Spectra were baseline-corrected against the cuvette with buffer alone. A $[\theta]_{222}$ value of $-33{,}000^\circ$ cm^2 dmol^{-1} was taken to correspond to 100% helix.[53]

Mutagenesis and detection of enriched SAMP2 conjugates

Plasmids pJAM117 and pJAM118 encoding Flag-tagged SAMP2 E53A and E53G variants were prepared using QuikChange Lightning site-directed mutagenesis kit (Stratagene, La Jolla, CA) with plasmid pJAM94931 as template and primers 1 (For_SAMP2 E53A, 5′-GAAGACCAGTCCGTCGCA GTCGACCGCGTGAAG-3′; Rev_SAMP2 E53A, 5′-C TTCACGCGGTCGACTGCGACGGACTGGTCTTC-3′) and primers 2 (For_SAMP2 E53G, 5′-GAAGACCAG TCCGTCGGAGTCGACCGCGTGAAG-3′; Rev_SAM P2 E53G, 5′-CTTCACGCGGTCGACTCCGACGGAC TGGTCTTC-3′), respectively. Mutation sites were verified by Sanger DNA sequencing (Eton Bioscience, San Diego, CA). Plasmids were isolated from *E. coli* GM2163 and transformed into *Hfx. volcanii* HM1041 (Δ*samp1*) cells as described previously.[36] *Hfx. volcanii* HM1041-pJAM949 (*samp2*) was used as a positive control and HM1–41-pJAM202c (empty vector) was used as a negative control. Cells were grown to stationary phase in ATCC 974 complete medium and harvested by centrifugation as described previously.[31] Cell pellets (corresponding to 0.065 OD_{600} units of cells per lane) were boiled in SDS-Laemmli buffer and separated by SDS-PAGE. The Flag-tagged proteins were detected by immunoblotting using alkaline phosphatase-linked anti-Flag M2 monoclonal antibody (Sigma, St. Louis, MO). The PVDF membranes were also stained with Ponceau S to confirm equal protein loading and transfer. Alkaline phosphatase activity was detected colorimetrically using nitroblue tetrazolium chloride and 5-bromo-4- and 5-bromo-4-chloro-3-indolyl phosphate and by chemiluminescence using CDP-Star (Life Technologies, Guilford, CT) with X-ray film (GE Healthcare).

Accession numbers

Coordinates and structure factors have been deposited in the Research Collaboratory for Structural Bioinformatics Protein Data Bank with accession numbers 4HRS (SAMP2) and 2M19 (HVO_2177). The resonance assignments of HVO_2177 have been deposited at the BioMagResBankII with entry code 18850.

Acknowledgments

The authors thank Wuxian Shi of the National Synchrotron Light Source X29A beamline for assistance with X-ray data collection and processing, Irina Bezsonova and Dmitry Korzhnev for fruitful discussions on NMR data collection and CS-Rosetta analysis, and Peter Setlow for critical reading of the manuscript. The authors declare no conflict interest.

References

1. Kerscher O, Felberbaum R, Hochstrasser M (2006) Modification of proteins by ubiquitin and ubiquitin-like proteins. Annu Rev Cell Dev Biol 22:159–180.
2. Hochstrasser M (2009) Origin and function of ubiquitin-like proteins. Nature 458:422–429.
3. Schwartz DC, Hochstrasser M (2003) A superfamily of protein tags: ubiquitin, SUMO and related modifiers. Trends Biochem Sci 28:321–328.
4. Welchman RL, Gordon C, Mayer RJ (2005) Ubiquitin and ubiquitin-like proteins as multifunctional signals. Nat Rev Mol Cell Biol 6:599–609.
5. Ciechanover A, Schwartz AL (2004) The ubiquitin system: pathogenesis of human diseases and drug targeting. Biochim Biophys Acta 1695:3–17.
6. Petroski MD (2008) The ubiquitin system, disease, and drug discovery. BMC Biochem 9:S7.
7. Dye BT, Schulman BA (2007) Structural mechanisms underlying posttranslational modification by ubiquitin-like proteins. Annu Rev Biophys Biomol Struct 36:131–150.
8. Pickart CM, Eddins MJ (2004) Ubiquitin: structures, functions, mechanisms. Biochim Biophys Acta 1695:55–72.
9. Kraulis PJ (1991) Similarity of protein G and ubiquitin. Science 254:581–582.

10. Pickart CM (2001) Mechanisms underlying ubiquitination. Annu Rev Biochem 70:503–533.
11. Volker C, Lupas AN (2002) Molecular evolution of proteasomes. Curr Top Microbiol Immunol 268:1–22.
12. Maupin-Furlow J (2012) Proteasomes and protein conjugation across domains of life. Nat Rev Microbiol 10: 100–111.
13. Darwin KH (2009) Prokaryotic ubiquitin-like protein (Pup), proteasomes and pathogenesis. Nat Rev Microbiol 7:485–491.
14. Chen X, Solomon WC, Kang Y, Cerda-Maira F, Darwin KH, Walters KJ (2009) Prokaryotic ubiquitin-like protein pup is intrinsically disordered. J Mol Biol 392: 208–217.
15. Liao S, Shang Q, Zhang X, Zhang J, Xu C, Tu X (2009) Pup, a prokaryotic ubiquitin-like protein, is an intrinsically disordered protein. Biochem J 422:207–215.
16. Sutter M, Striebel F, Damberger FF, Allain FH, Weber-Ban E (2009) A distinct structural region of the prokaryotic ubiquitin-like protein (Pup) is recognized by the N-terminal domain of the proteasomal ATPase Mpa. FEBS Lett 583:3151–3157.
17. Pearce MJ, Mintseris J, Ferreyra J, Gygi SP, Darwin KH (2008) Ubiquitin-like protein involved in the proteasome pathway of *Mycobacterium tuberculosis*. Science 322:1104–1107.
18. Burns KE, Liu WT, Boshoff HI, Dorrestein PC, Barry CE, 3rd (2009) Proteasomal protein degradation in *Mycobacteria* is dependent upon a prokaryotic ubiquitin-like protein. J Biol Chem 284:3069–3075.
19. Striebel F, Imkamp F, Sutter M, Steiner M, Mamedov A, Weber-Ban E (2009) Bacterial ubiquitin-like modifier Pup is deamidated and conjugated to substrates by distinct but homologous enzymes. Nat Struct Mol Biol 16:647–651.
20. Sutter M, Damberger FF, Imkamp F, Allain FH, Weber-Ban E (2010) Prokaryotic ubiquitin-like protein (Pup) is coupled to substrates via the side chain of its C-terminal glutamate. J Am Chem Soc 132:5610–5612.
21. Iyer LM, Burroughs AM, Aravind L (2006) The prokaryotic antecedents of the ubiquitin-signaling system and the early evolution of ubiquitin-like beta-grasp domains. Genome Biol 7:R60.
22. Hochstrasser M (2000) Evolution and function of ubiquitin-like protein-conjugation systems. Nat Cell Biol 2:E153–E157.
23. Wang C, Xi J, Begley TP, Nicholson LK (2001) Solution structure of ThiS and implications for the evolutionary roots of ubiquitin. Nat Struct Biol 8:47–51.
24. Rudolph MJ, Wuebbens MM, Rajagopalan KV, Schindelin H (2001) Crystal structure of molybdopterin synthase and its evolutionary relationship to ubiquitin activation. Nat Struct Biol 8:42–46.
25. Goehring AS, Rivers DM, Sprague GF, Jr. (2003) Urmylation: a ubiquitin-like pathway that functions during invasive growth and budding in yeast. Mol Biol Cell 14:4329–4341.
26. Leidel S, Pedrioli PG, Bucher T, Brost R, Costanzo M, Schmidt A, Aebersold R, Boone C, Hofmann K, Peter M (2009) Ubiquitin-related modifier Urm1 acts as a sulphur carrier in thiolation of eukaryotic transfer RNA. Nature 458:228–232.
27. Schlieker CD, Van der Veen AG, Damon JR, Spooner E, Ploegh HL (2008) A functional proteomics approach links the ubiquitin-related modifier Urm1 to a tRNA modification pathway. Proc Natl Acad Sci USA 105: 18255–18260.
28. Darwin KH, Hofmann K (2010) SAMPyling proteins in archaea. Trends Biochem Sci 35:348–351.
29. Makarova KS, Koonin EV (2010) Archaeal ubiquitin-like proteins: functional versatility and putative ancestral involvement in tRNA modification revealed by comparative genomic analysis. Archaea 2010. Article ID 710303. doi: 10.1155/2010/710303.
30. Miranda HV, Nembhard N, Su D, Hepowit N, Krause DJ, Pritz JR, Phillips C, Soll D, Maupin-Furlow JA (2011) E1- and ubiquitin-like proteins provide a direct link between protein conjugation and sulfur transfer in archaea. Proc Natl Acad Sci USA 108:4417–4422.
31. Humbard MA, Miranda HV, Lim JM, Krause DJ, Pritz JR, Zhou G, Chen S, Wells L, Maupin-Furlow JA (2010) Ubiquitin-like small archaeal modifier proteins (SAMPs) in *Haloferax volcanii*. Nature 463:54–60.
32. Hepowit NL, Uthandi S, Miranda HV, Toniutti M, Prunetti L, Olivarez O, De Vera IM, Fanucci GE, Chen S, Maupin-Furlow JA (2012) Archaeal JAB1/MPN/MOV34 metalloenzyme (HvJAMM1) cleaves ubiquitin-like small archaeal modifier proteins (SAMPs) from protein-conjugates. Mol Microbiol 86:971–987.
33. Ranjan N, Damberger FF, Sutter M, Allain FH, Weber-Ban E (2011) Solution structure and activation mechanism of ubiquitin-like small archaeal modifier proteins. J Mol Biol 405:1040–1055.
34. Jeong YJ, Jeong BC, Song HK (2011) Crystal structure of ubiquitin-like small archaeal modifier protein 1 (SAMP1) from *Haloferax volcanii*. Biochem Biophys Res Commun 405:112–117.
35. Shen Y, Lange O, Delaglio F, Rossi P, Aramini JM, Liu G, Eletsky A, Wu Y, Singarapu KK, Lemak A, Ignatchenko A, Arrowsmith CH, Szyperski T, Montelione GT, Baker D, Bax A (2008) Consistent blind protein structure generation from NMR chemical shift data. Proc Natl Acad Sci USA 105:4685–4690.
36. Dyall-Smith M (2009) The Halohandbook: protocols for Halobacterial genetics. Available from: www.haloarchaea.com/resources/halohandbook/Halohandbook_2009_v7.1.pdf.
37. Cunningham BC, Wells JA (1989) High-resolution epitope mapping of hGH-receptor interactions by alanine-scanning mutagenesis. Science 244:1081–1085.
38. Yan BX, Sun YQ (1997) Glycine residues provide flexibility for enzyme active sites. J Biol Chem 272:3190–3194.
39. Hartman AL, Norais C, Badger JH, Delmas S, Haldenby S, Madupu R, Robinson J, Khouri H, Ren Q, Lowe TM, Maupin-Furlow J, Pohlschroder M, Daniels C, Pfeiffer F, Allers T, Eisen JA (2010) The complete genome sequence of *Haloferax volcanii* DS2, a model archaeon. PLoS One 5:e9605.
40. Shen Y, Delaglio F, Cornilescu G, Bax A (2009) TALOS+: a hybrid method for predicting protein backbone torsion angles from NMR chemical shifts. J Biomol NMR 44:213–223.
41. Guntert P (2004) Automated NMR structure calculation with CYANA. Methods Mol Biol 278:353–378.
42. Brunger AT, Adams PD, Clore GM, DeLano WL, Gros P, Grosse-Kunstleve RW, Jiang JS, Kuszewski J, Nilges M, Pannu NS, Read RJ, Rice LM, Simonson T, Warren GL (1998) Crystallography & NMR system: a new software suite for macromolecular structure determination. Acta Crystallogr D Biol Crystallogr 54:905–921.
43. Holm L, Kaariainen S, Rosenstrom P, Schenkel A (2008) Searching protein structure databases with DaliLite v.3. Bioinformatics 24:2780–2781.
44. Huang DT, Hunt HW, Zhuang M, Ohi MD, Holton JM, Schulman BA (2007) Basis for a ubiquitin-like protein thioester switch toggling E1-E2 affinity. Nature 445: 394–398.

45. Duda DM, Borg LA, Scott DC, Hunt HW, Hammel M, Schulman BA (2008) Structural insights into NEDD8 activation of cullin-RING ligases: conformational control of conjugation. Cell 134:995–1006.
46. Otwinowski Z, Minor W (1997) Processing of X-ray diffraction data collected in oscillation mode. Methods Enzymol 276:307–326.
47. McCoy AJ (2007) Solving structures of protein complexes by molecular replacement with Phaser. Acta Crystallogr D Biol Crystallogr 63:32–41.
48. Winn MD, Murshudov GN, Papiz MZ (2003) Macromolecular TLS refinement in REFMAC at moderate resolutions. Methods Enzymol 374:300–321.
49. Davis IW, Leaver-Fay A, Chen VB, Block JN, Kapral GJ, Wang X, Murray LW, Arendall WB, 3rd, Snoeyink J, Richardson JS, Richardson DC (2007) MolProbity: all-atom contacts and structure validation for proteins and nucleic acids. Nucleic Acids Res 35:W375–W383.
50. Hoch JC, Stern AS (1996) NMR data processing. New York: Wiley-Liss.
51. Bartels C, Xia TH, Billeter M, Guntert P, Wuthrich K (1995) The program XEASY for computer-supported NMR spectral analysis of biological macromolecules. J Biomol NMR 6:1–10.
52. Laue TM, Shah BD, Ridgeway TM, Pelletier SL, Computer-aided interpretation of analytical sedimentation data for proteins. In: Harding S, Rowe A, Horton J, Eds. (1992) Analytical ultracentrifugation in biochemistry and polymer science. Cambridge, United Kingdom: Royal Society of Chemistry, pp 90–125.
53. Chen YH, Yang JT, Chau KH (1974) Determination of the helix and beta form of proteins in aqueous solution by circular dichroism. Biochemistry 13:3350–3359.